Simple Three-layer Pagoda Analysis

Haoyu Liang, Jian Chen & Gregory MacRae
University of Canterbury, Christchurch, New Zealand.

Minghao Li
University of British Columbia, Vancouver, Canada.

Liang-Jiu Jia
Tongji University, Shanghai, China.

ABSTRACT

This paper describes the construction of a simplified three-storey pagoda and its behaviour. The following are developed: (i) a 1/20 scale 3-D printed overall structure model, (ii) a 1/10 scale 3-D printed model of one *dougong* joint, (iii) a numerical model which is subjected to a lateral force distribution and an earthquake record, (iv) element free-body forces, (v) element capacities considering material properties expected for old Chinese structures, wood grain direction, and the different failure modes, and (vi) a comparison between element demands and capacities due to earthquake shaking.

The 3-D printed models enabled an understanding of the construction methods, and the way this system carries gravity and lateral forces without any special fasteners. The structure numerical model developed using SAP2000 had a period of 0.49s. When the structure is subjected to an inverted triangular force distribution, the uplift occurred between the first and second stories at a roof displacement of 6 mm when the base shear coefficient was 0.66 and the drift ratio was 1%. At an uplift of 10 mm with a base shear coefficient and roof drift ratio were 1.26 and 2% respectively. Time history analysis, with the Altadena Eaton Canyon Park 1991 ground motion record N-S component scaled so that the spectral acceleration at that period is the same as that expected for a 500-year event in Christchurch structure assuming soil class D and 5% damping gave maximum storey drift, roof drift, and uplift displacement of 1.11%, 0.58%, and 6.8mm respectively. Considering the different components and modes, the maximum force demand capacity ratio was 0.21 in the second-storey lower beam considering the compression failure mode.

1 INTRODUCTION

Ancient wooden pagodas have been constructed in China for hundreds of years. They have been used as religious gathering places, as centres for community gatherings, as status symbols indicating power and

prestige, and as towers for surveillance, and protection in times of war. They use *dougong* (interlocking wooden bracket) construction without fasteners (such as nails, bolts, ropes, or straps). Many of these pagodas remain in use today, even though they have been subject to a wide variety of loading types including snow, wind, earthquake, a range of temperatures and humidity, and in some cases even cannon fire. While there has been a renewed interest in pagodas, simple descriptions of the mechanisms by which they carry forces, and their factors of safety against collapse, are not available.

In order that pagodas can continue to be built, while providing significant safety under expected loads, there is a need to both understand their construction, and their likely seismic performance.

This paper seeks to address these needs for a simplified 3-storey forked column-type pagoda by seeking answers to the following questions:

a) How are such pagodas constructed?

b) What are the deformation modes under significant lateral displacement?

c) What are the demand-to-capacity ratios for different modes of failure under design-level earthquake shaking?

2 LITERATURE

Pagodas are of different forms, and several studies have been conducted to understand their construction. This has enabled the construction of many modern pagodas particularly throughout Asia. Often, they are constructed in stories that simply sit on top of each other. Stories hidden by the roof are often braced. The weakest location of the members is generally inside the joint. Elements of a structure and joint are shown in Figure 1 (Fu, 2009). Deformation may occur by storey rocking if member failure at a connection does not occur first. A few studies in English describe the construction, and the *dougong* joint (E.g., Xie et al., 2020, Xue et al., 2022, and Zhang, et. al., 2022). Often, at the ground level, the columns simply sit on the ground, sometimes without even a shear key. A few studies (Sun et al. 2022) have described the seismic performance of pagodas, however, generally the deformation modes and safety factors are not explained clearly.

One notable wooden pagoda is that at Yingxian as shown in Figure 1. It is 67.3 m high, with an octagonal plan and a base diameter of 30.3 m. The appearance of the wooden pagoda is five layers, but inside the pagoda, there are four hidden layers within the roof stories, resulting in a total of nine layers. The tower was built entirely of red pine wood. The volume of timber is 3,000 m³ weighing about 2,600 tons (Li, 2019)

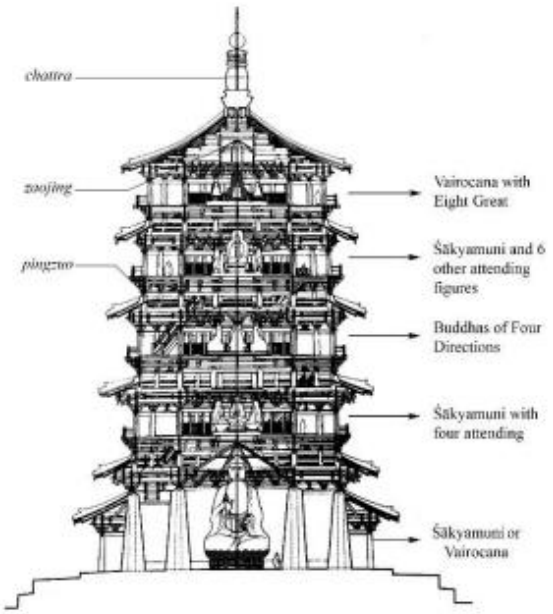

Figure 1: Yingxian Pagoda (Fu, 2009)

A simple model tested at Tongji University (Jia, 2022) was based on the Guanyin Pagoda in Tianjin. The Tongji model second storey has a complex bracing wall on the longer beam side and only a single diagonal brace on the shorter beam side, which could create large torsion and make the building more vulnerable to damage. This is not realistic of actual pagodas, but it was suitable for their one-directional shaking test.

In traditional Chinese buildings, the connection between building and the foundation is usually connected by inserting a projecting piece at the base of the column into the concave part of the column base. This limits the lateral movement of the column but allows rotation like a pinned support.

3 METHODOLOGY

3.1 Modelling Considerations

The simplified pagoda considered in this project is shown in Figure 2. The material considered is red beech. The height is 6.9m, the span of the long and short sides are 3.7m, and 1.9m respectively. The storey heights are 3.3m, 2.13m and 2.13m up the height. It is based on the Tongji model (Jia, 2022) but has been simplified to use 2-layer *dougong* joints, rather than the 5-layers of wood used in practice. Bracing is placed on both sides of the structure to increase realism and avoid torsional issues. The braces, placed in a V shaped configuration in the hidden levels, pierce the beams and columns that hold them in position.

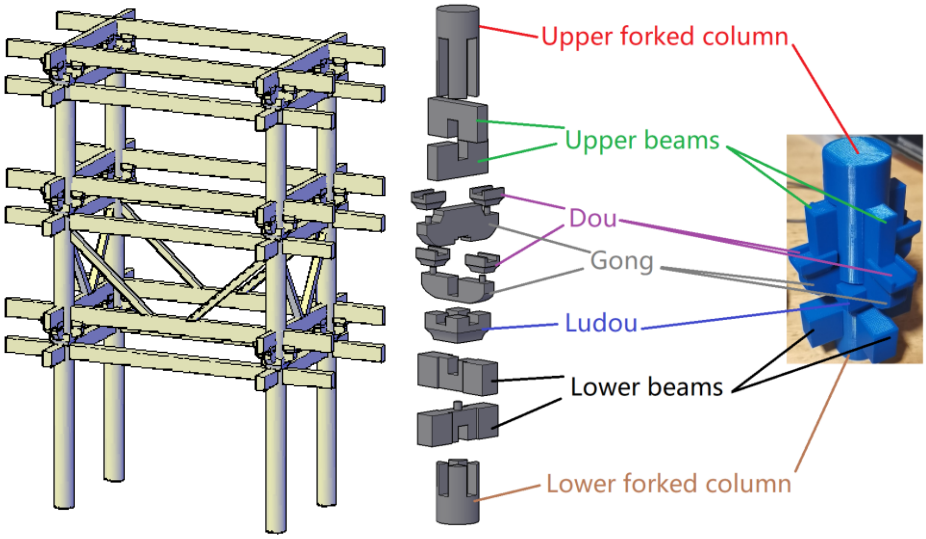

Figure 2 and 3: Pagoda model analysed (from CAD) (Left); Detailed diagram of the Dougong set (Right)

The *dougong* joint provides moment capacity thereby limiting the lateral movement of each floor. The critical element of this structure is the forked column. The beam is inserted into the forked column recess to prevent beam lateral movement and to maintain inter-floor connectivity (Jia, 2022). In the joint, because of erection tolerances, some relative sliding of elements can occur, and this can dissipate some energy. Gravity holds the joint elements together. If member failure within the joint does not occur, then rocking can occur causing uplift between stories. When rocking occurs, gravity forces act on the column and *dougong* on the compression side of the building.

Two physical models used to understand the construction method and mechanical behaviour of the pagoda was 3D printed using PLA+ (a kind of plastic filament material used in 3D printing), with a fill rate of 65%.

Demands and capacities are computed for (i) axial force, (ii) bending moment, and (iii) shear force, considering all possible failure modes within the connection zone acknowledging the grain direction. A timber self-weight of 11 kN/m² was used in the calculations (Li, 2019). Within the joint, strengths relate to the actual forces on the shaped-down members. Timber element strength modifications were ignored. An example beam capacity calculation is shown below. The grain is in the direction of the beam and force is applied transverse to the member.

$f_b = 116$ MPa	bending strength
$f_c = 54$ MPa	compression strength
$f_s = 13.6$ MPa	shear strength
$b = 150mm$	beam breadth
$d = 200mm$	beam depth
$Z = b * d^2/6 = 0.001m^3$	section modulus
$A = b * d = 0.03m^2$	cross-sectional area
$M_n = f_b * Z = 116kNm$	bending capacity
$V_n = f_s * A = 408kN$	section shear capacity (conservative)
$N_c = f_c * A = 1.62 * 10^3 kN$	axial capacity

Element capacity is calculated as the shear, bending and axial load capacity of (i) the entire member, and (ii) at the member end connection. The tension and shear strength along likely failure planes, including those parallel to the grain, were used.

3.2 Numerical Model

A numerical 2D frame model was made of a frame with the short beam span in Figure 2. The frame was 6.9m tall. This global model did not consider joint details. Pinned connections were considered at the column bases. The upper beams stand on the *dou*, as shown in Figure 3. The *dou* is connected to the *gong* by means of pins, and the forked columns secure the upper beams and *gong* to the *ludou*. The components use mortise and tenon connections without fasteners. The gap element is used to model joints under tension. As the model is simplified, the number of components in the actual building far exceeds the number of components in the model. Therefore, based on the data for the Yingxian wooden pagoda, the estimated weight of the building is 11 kN/m², so an additional 1.6 tonnes per storey is required to meet the weight of the actual building.

The model was subjected to pushover tests under an inverted triangular distribution of forces to a 4% drift ratio and base shear and roof displacements were recorded. A time history analysis was also conducted, with the Altadena Eaton Canyon Park 1991 ground motion record N-S component scaled so that the spectral acceleration at the structural period is the same as that expected for a 500-year event in Christchurch structure assuming soil class D and 5% damping. The damping ratio used for the analysis was 4%, in all modes with initial stiffness proportional damping. The integration timestep was 0.02s and Newmark-β integration was used with $\beta = 0.25$.

If no element failure occurs, then the expected deformation mode is rocking, as shown in Figure 4.

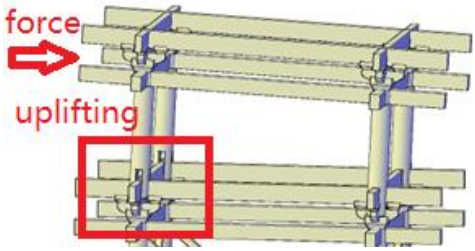

Figure 4: Storey Rocking Example

4 BEHAVIOUR

4.1 Physical Model and Load Paths

Two 3D printed physical models, at a scale of 1:10 for the joint, and 1:20 for the overall structure, are shown in Figures 5 and 6 respectively. These two models show how the pagoda is constructed, and the mechanical behaviour of the structure when subjected to different forces.

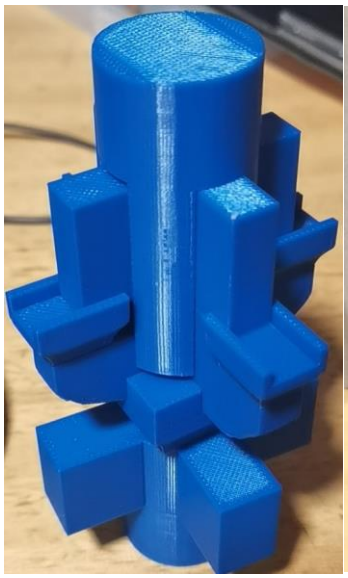

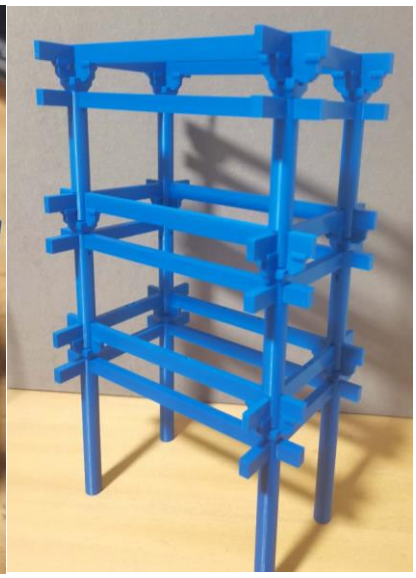

Figure 5: 3D printed model of a typical joint *Figure 6: 3D printed model of the pagoda (Right)*

Figure 7. Shows more details on how the beams and columns are connected. At the top of the lower column the beams can bear against the column and the cross beam. However, at the bottom of the top column, it can bear against the cross beam only.

(a) Bottom of Upper Column *(b) Top of Lower Column*

Figure 7. Beam-column connection horizontal cross-sections

The connection between the top of the lower column and the beams is more complicated than the connection between the beams and the bottom of the upper columns. Figure 8 shows member connection forces for some cases. The red lines indicate the locations where the beam bears against the column, and the purple lines indicate where it can bear against the crossbeam. The beam axial force equilibrates the column base shear reaction and can be understood by considering a free-body diagram of one-half of the frame.

In Figure 8a, for an lower beam with a downward beam shear, ignoring compression zones, where high compressive forces can occur without system failure, the failure major beam failure modes are (a) flexure and shear in the reduced section, and horizontal delamination due to shear in the parallel to the grain. However, this later mechanism will not occur if the length of beam past the reduced section is long enough (as is assumed in the analyses).

In Figure 8b, where the beam shear is upward, a vertical downward gravity or force is required for equilibrium. If that force is not present, then vertical sliding of the beam in that location can occur. This does not cause failure, but it does decrease the vertical upward force, and hence the moment, that can be applied. Apart from this, the forces are similar to that in Figure 8a.

The upper beams, the force distributions shown in Figures 8c and 8d, and the explanations are similar to those for the lower beams.

Figures 8e-h show the forces on the column from Figures 8a-h respectively. It may be seen in Figure 8e, that two load paths are shown for the lateral force applied at the top of the quadrant (i.e. quarter of a circle) section cantilevers on one side of the column. One is direct to the base of the figure shown. The other passes through the material placed within the column. It is activated only when there is a close fit between these elements and the quadrant upstands, and when there is significant friction. In either case, it may be seen that the applied compressive forces on the top of the outstand cause tension on the outside of the quadrant and column. If tension were applied on the inside of the quadrant and column, there would be a tendency for vertical splitting, parallel to the grain, to occur at the base of the quadrant shaped cantilevers. This case is avoided protecting the column against this failure mode. Because of these modes of force transfer, the failure of the column in this connection area has been ignored in this study.

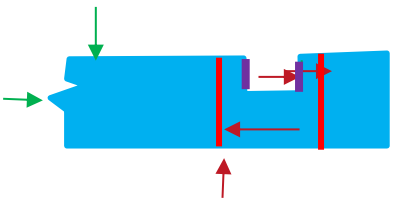

(a) Lower beam under vertical downward force

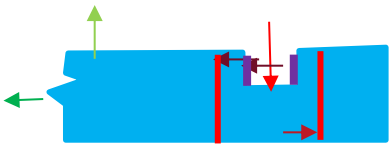

(b) Lower beam under vertical upward force

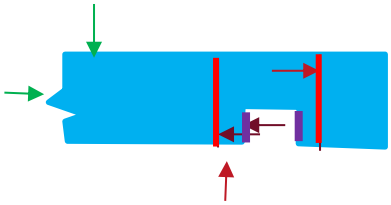

(c) Upper beam under vertical downward force

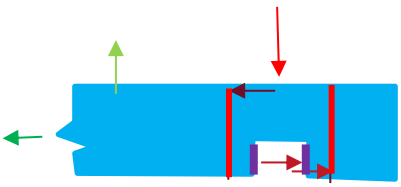

(d) Upper beam under vertical upward force

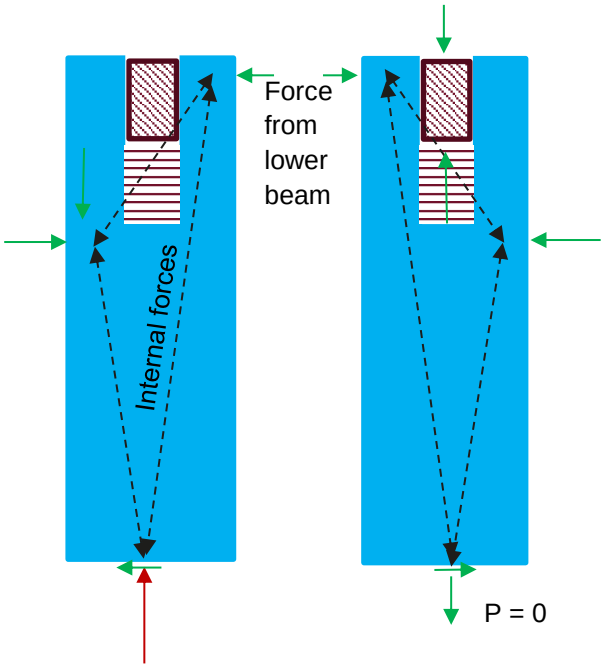

(e) Column forces for a *(f) Column forces for b*

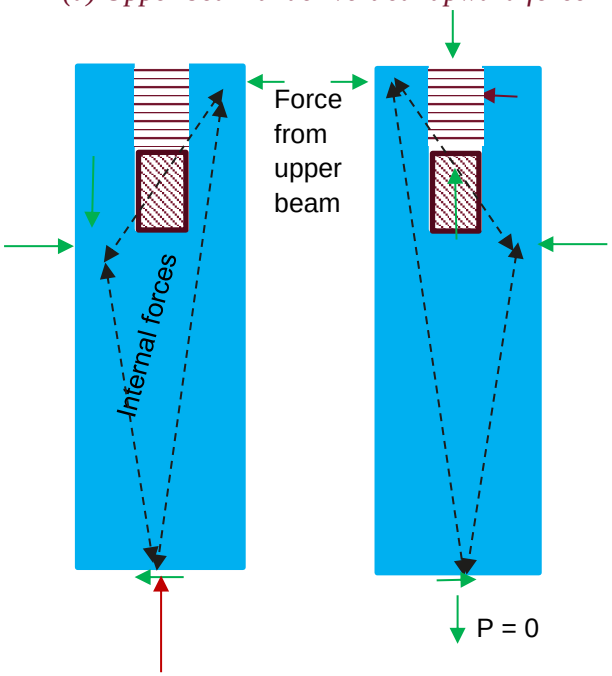

(g) Column forces for c *(h) Column forces for d*

Figure 8. Example of force distribution at upper end of column (not to scale)

The values of the forces obtained in Figures 8a-d may be found from equilibrium. It is assumed that the location of the centroids of horizontal reaction forces within the beam are applied at 0.05 times the beam

depth from the external edge. In Figure 8a, the applied vertical force at the top left of the beam is given as the beam moment at the column face divided by the distance to the point of contraflexure. This is also equal to the column face beam shear. Then, the vertical reaction from the column at the column face is equal to this. By taking a free body diagram about the right hand side of the beam, the horizontal force on the upper right is equal to the moment at the column face, divided by the distance between the horizontal forces at the end of the beam, which is 0.9 times the beam depth. Another way of looking at this is by considering the moment at the centre of the beam at the column face, and then dividing this by the force couple = (0.45x F + 0.45F) = 0.9F, where F is the horizontal force toward the right at the top of the beam cut out. It may be noted that the beam force toward the left has a magnitude equal to this value plus the beam axial force. The beam axial force is equal to the column shear.

The moment demand in the reduced section of the beam, shown in Figure 8a, may be found as the horizontal force pushing against the end of the beam within the cut-out, multiplied by the distance from the force to the centre of the reduced section of the beam. The stress demand is then computed as the moment divided by the beam reduced section elastic modulus. The moments and stresses for the situations described in Figure 8d is similar, while those from Figures 8b and c are less critical.

Similar considerations for the lower end of the column can also be made, but these are not shown here. One of the major differences is that an upside-down version of the upper end of the column would not work, as the beams would want to fall out as a result of gravity. The beams at the upper column base, and the upper columns themselves, are therefore supported by the *dougong* structure. Another difference is that the beams are not wider than the gap between the quadrant outstands as shown in Figure 7a. Beam flexure is therefore transferred to the cross beam, rather than to the column. This is not likely to be a major issue because there is not expected to be much moment demand at this location because the bottom of the *dou* is pinned in implying zero moment there, and low moments nearby.

4.2 Demand-to-Capacity Ratios

For the conceptual model, some computed member capacities are given in Table 1. It may be seen that the strengths at the member ends are often significantly less than those along the main part of the member. Also, storey shear demands at 2 different drift levels are given in Table 2. For simplicity, only the configuration in Figure 7b were considered. The resistance of the Figure 7a configuration is decreased because the beam width is less and there is no bearing directly on the column, but interaction with the *dougong* can increase the capacity there.

Table 1: Member Capacities

	Shear Capacity	Bending Capacity	Axial Load Capacity
Column	961kN	308kNm	961kN
Upper beam	340kN	120.8kNm	1350 kN
Lower beam	408kN	116kNm	1620 kN
Gong	292kN	66kNm	1158kN
Dou	583kN	110kNm	1367kN
Column (each quadrant)	60.1kN	6.3kNm	239kN
Upper Beam (half)	204kN	29kNm	810kN
Lower Beam (half)	170kN	30.2kNm	675kN

Table 2: Storey shear forces

Level	1% Drift (kN)	2% Drift (kN)	Seismic load (kN)
Roof	16.7	31.7	13.6
2	10.1	19.3	8.3
1	6.27	12	5.1
Total	33	63	27

Gravity demands were not larger than 10% of the capacity of any structural element and therefore do not critically affect the structural behaviour. Under lateral force, computed demand-to-capacity ratios were generally greater for the *dougong* and for the column fork, than for the flexural, axial and shear demands in the beams and columns.

The base shear force when uplift occurred at the base of the structure. It was 50.8kN at a roof drift ratio of about 1.6%. After uplift, the base shear remained approximately constant as the system rocked.

From elastic response calculations at a 2% roof drift ratio (assuming no uplift), the largest shear force and bending moment demands occurred at the top of the ground storey compression column being 78.7kN and 31.5kNm. The capacities were 961kN and 308 kNm respectively indicating that no failure was expected. The maximum beam bending moment and shear force were 71.5 kNm and 75.2 kN respectively also being lower than the capacities of 116kNm and 408kN. The maximum vertical axial force demand of 196 kN was less than the column end capacity of 240 kN.

At the reduced section of the beam, bending moment demands were 24.6 kNm, 30 kNm, and 55.6 kNm, from analysis considering the Christchurch design base shear force which corresponded to 0.8% drift, 1% roof drift and 2% roof drift respectively. The moment demands at uplift, corresponding to 1.6% drift was 46.3kNm. The capacity computed in Table 2 was 30.2kN indicating that failure of the connection is expected before rocking occurs. However, due to the level of shaking considered, that is associated with 0.8% drift, no beam failure within the connection is expected.

At larger drifts, failure could be expected, however this does not necessarily occur in reality because pagodas may:

i) have walls at the ground storey, made of brick or earth infill, which can increase the lateral capacity of the pagoda, and

ii) even if there are no walls at the ground (first) storey, the column bases may slide because there is often no shear key in the pedestal (or *zhuchu*) on which the structure sits.

For the upper stories, the capacity to demand ratios were less than unity. After uplift, the resistance of both the upper and lower beams at each level carry the moments, shears and axial demandsdue to the self-weight of their own storey. No forces greater than these can be caused in the rocking structure due to horizontal shaking.

4.3 Global Response

The time history analysis was conducted using the N-S component of the 1991 ground motion record from Altadena Eaton Gorge Park scaled to the 1 in a 500-year event in for a Christchurch structure, assuming a soil class of D and damping of 5%. Vertical and lateral displacements at each storey are shown in Figure 9 and Figure 10, respectively. Uplift only occurs in the upward connection as expected.

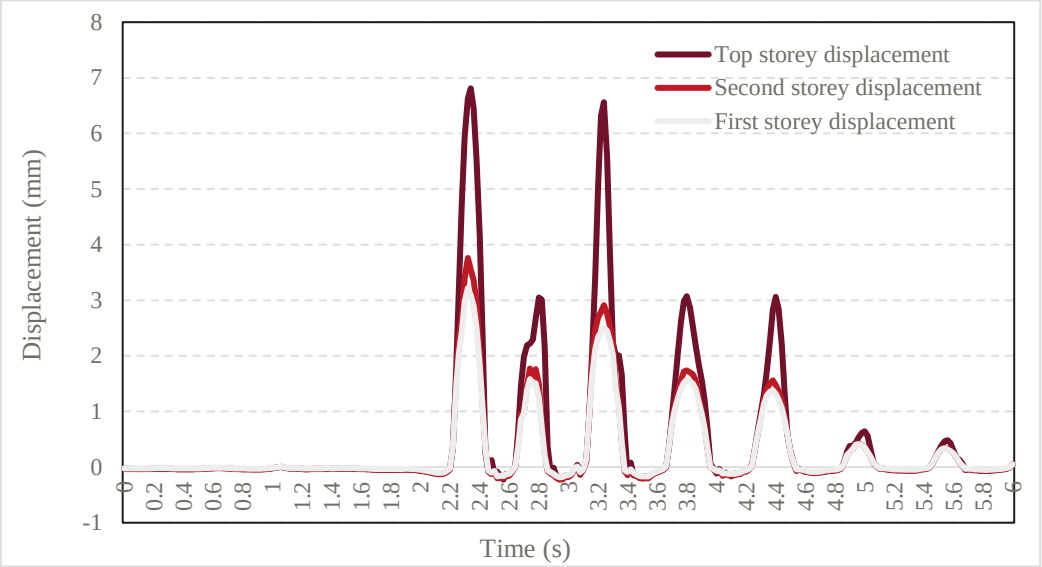

Figure 9: Floor vertical displacements on left hand side (Record = Altadena – Eaton Canyon Park at N-S component, Damping = 4%)

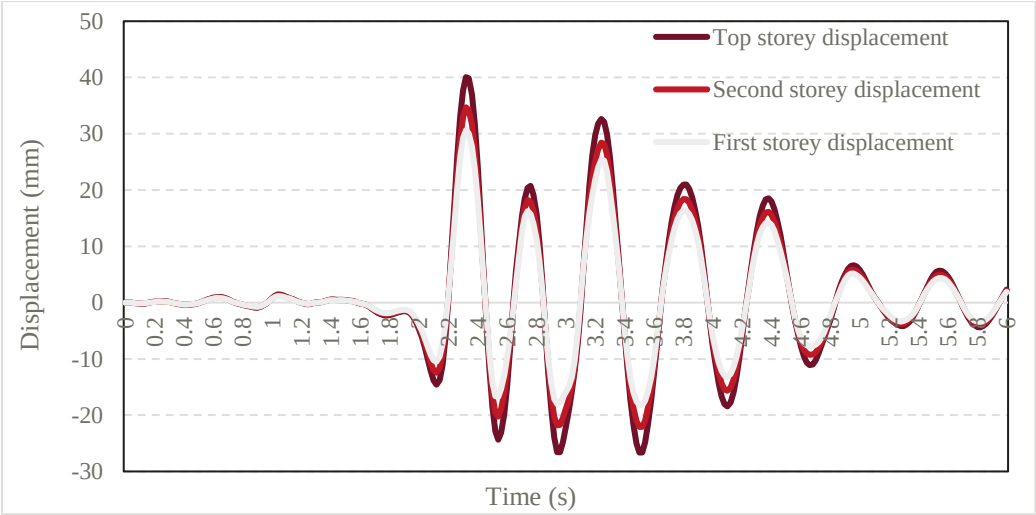

Figure 10: Floor lateral displacements (Record = Altadena – Eaton Canyon Park at N-S component, Damping = 4%)

5 CONCLUSIONS

Through the procedures of designing models, printing models, theoretical calculations, and computer simulations, it was shown that:

a) Pagodas are constructed by the fitting together of wooden elements without nails or rope. At the joint, where the element sizes are smallest, is where failure is expected. Each level sits on top of the level below and can rock. Braced levels are often hidden by the roof. *Dougong* (interlocking wooden bracket) joints can provide moment resistance at column ends.

b) Lateral forces carried by the braces in the braced stories, and in moment action in unbraced stories because of the *dougong* joints. Rocking can occur between levels.

c) Under earthquake shaking similar to that for the 500-year in Christchurch, the element capacities were not reached. However, for higher levels of shaking, in this particular design, failure within the beam reduced section of the joint was expected before rocking occurred.

6 ACKNOWLEDGMENTS

The authors would like to express grateful appreciation to Minghao Li for helping with the project, to Liangjiu Jia for providing the original model and help, to Humayun Khan and Alan Poynter for helping with the 3D printing, and to Zheng Luo for helping with the Sap2000 modelling.

7 REFERENCES

Fu, X., 2009, Zhongguo gudai jianzhushi: Liangjin, Nanbeichao, Sui-Tang, Wudai, figure 121-4.

Te namu Timber (2022) Red Beech Technical Information, https://tenamutimber.co.nz/technical-information/red-beech/, (accessed 16 October 2022).

M. Stibor, P. Frantík. (2015) STRIAN online structural analyser, https://structural-analyser.com/(accessed 18 October 2022).

Xie, Q., Wang, L., Zhang, L., Xiang, W., and Hu W. 2020. Rotational Behaviour of Fork-Column Dou-Gong: Experimental Tests and Hysteresis Model. https://ascelibrary.org/doi/10.1061/%28ASCE%29CF.1943-5509.0001426.

Xue, J., Liang, X., Wu, C., Song, D. and Qi, L. 2022. Experimental and numerical study on eccentric compression performance of Dou-Gong brackets at column tops. https://www.sciencedirect.com/science/article/abs/pii/S2 352012421010924?via%3Dihub

Zhang, B., Xie, Q., Li, S., Zhang, L. and Wu, Y. 2022. Structural performance of Dou-Gong brackets of Yingxian Wood Pagoda under vertical load – An experimental study. https://www.sciencedirect.com/science/article/abs/pii/S0 141029622003601?via%3Dihub

L. Jia. (2022) Personal Communication. Lecturer, College of Civil Engineering, Tongji University, 5 Aug.

Z, Sun, P, Xiang, L, Jia, and R, Zhang. 2022. Seismic response and kinematic mechanisms of single-story pavilion-type timber frame based on shaking table test. https://www.sciencedirect.com/science/article/abs/pii/S2352012422009122

8 APPENDIX

Appendices, containing calculation details, scaled 3D CAD models, Sap2000 files, etc., are at this site:

https://www.dropbox.com/sh/ty7blw9pvid0aj5/AAAtdqmuMXFM4eBO68eMrk4wa?dl=0